

1    **A new approach to ecosystem disturbance detection  
2    and attribution (*disturbr*) using temporal and spatial  
3    information**

4    Annie C. Smith<sup>1,4</sup>, Zhihua Liu<sup>2,3</sup>, Phoebe L. Zarnetske<sup>1</sup>, Ashley P. Ballantyne<sup>3</sup>

5    <sup>1</sup>Michigan State University, East Lansing, MI 48824

6    <sup>2</sup>CAS Key Laboratory of Forest Ecology and Management, Institute of Applied Ecology,  
7    Chinese Academy of Sciences, Shenyang, 110016, China

8    <sup>3</sup>University of Montana, Missoula, MT 59812

9    <sup>4</sup>Corresponding Author: coope378@msu.edu

---

10 **Abstract**

11 Disturbance is a critical process for shaping ecological patterns and processes, including  
12 biodiversity, carbon and nutrient cycling, and ecosystem-climate feedbacks. Accurate as-  
13 sessments of current and future disturbance characteristics and trends are essential for un-  
14 derstanding the ecological processes and interactions within and among landscapes. Current  
15 methods for disturbance detection tend to rely on thresholds of time series change. How-  
16 ever, the accuracy of threshold-based methods often declines when applied to new regions.  
17 To develop more robust techniques of disturbance attribution and detection that can be  
18 transferred among regions, we developed *disturbr*, an approach that utilizes both temporal  
19 and spatial information with Random Forest machine learning. Variables in the Random  
20 Forest models include characteristics of single pixel time series in addition to spatial sum-  
21 maries of time series over several surrounding pixels. We assessed the ability of *disturbr* to  
22 detect and attribute forest disturbances on seven Landsat scenes, spanning a wide range of  
23 ecoregions in the United States, over seventeen years. We found that *disturbr* was as accu-  
24 rate as previous methods (overall kappa accuracy =  $76 \pm 8\%$ ; 8 – 25% false positive rate;  
25 1 – 19% false negative rate), and maintained that accuracy across regions. The inclusion  
26 of model predictor variables based on both temporal (single pixel) and spatial (neighboring

27 pixel) time series characteristics allowed us to determine the relative influence of temporal  
28 and spatial predictors in distinguishing disturbed from undisturbed locations. In the seven  
29 Landsat scenes, temporal predictors explained more variation in detection, and spatial pre-  
30 dictors explained more variation in attribution. However, despite their lower importance in  
31 the detection models, the inclusion of spatial predictors did result in a substantial improve-  
32 ment in model accuracies. In summary, our analysis shows that *disturbr* may have several  
33 advantages over existing techniques: (1) it uses spatial information to detect and attribute  
34 forest disturbance; (2) it enables attribution of specific disturbance types; and (3) it is trans-  
35 ferable across multiple ecoregions. This new method increases our ability to study current  
36 and future disturbance characteristics and trends by providing a new open source method  
37 for locating and attributing disturbances at local to regional scales.

38 **1 Introduction**

39 Disturbance is a critical process for shaping a multitude of ecological patterns and pro-  
40 cesses. For example, disturbances maintain and change species assemblages and biodiversity  
41 (Frissell 1973, Smucker et al. 2005), alter consumer-resource systems (Yensen et al. 1992),  
42 shift soil carbon and nitrogen pools and cycling (Wan et al. 2001, Morehouse et al. 2008),  
43 and lead to climate feedbacks (Maness et al. 2013, Cooper et al. 2017, Liu et al. 2019). Dis-  
44 turbance regime characteristics (e.g., frequency, severity, and extent) influence the patterns  
45 of these impacts and are responsible for many of the differences in patterns and functions  
46 among ecosystem types. Therefore, accurate assessments of current and future disturbance  
47 regime characteristics and trends are essential for understanding the ecological processes and  
48 interactions within and among landscapes (McDowell et al. 2015). In order to address this  
49 need, many methods have been developed to detect and attribute disturbances using satellite  
50 imagery. However, the accuracies of existing methods vary depending on ecosystem and dis-  
51 turbance type. Additionally, current approaches of detection and attribution often involve  
52 several computing platforms making it difficult to apply a detection algorithm across several  
53 systems with consistent accuracy. We aim to improve the transferability and efficiency of  
54 detection and attribution methods while maintaining high accuracy.

55 Most current methods to detect forest disturbances use time series modeling or temporal  
56 decomposition on individual pixels (pixel of interest; POI) in order to detect when distur-  
57 bances occur across landscapes (e.g., Kennedy et al. 2010, Verbesselt et al. 2010, Zhu et al.  
58 2012). These temporal approaches work well when applied to regions for which they have  
59 been tuned, but their accuracy declines when applied to new areas (Cohen et al. 2017). Addi-  
60 tionally, the temporal approaches require a separate method to be applied after the detection  
61 process in order to attribute the detected disturbances. Previous research has mentioned the  
62 potential for spatial information to improve detection and attribution methods (Rich et al.  
63 2010). While several studies have used neighborhood pixel information (NPI) to attribute  
64 disturbances once detected using a temporal POI approach (Kennedy et al. 2015, Shimizu

65 et al. 2017, Zhao et al. 2018), none have used spatial information simultaneously for both  
66 disturbance detection and attribution. The incorporation of spatial data (e.g., NPI) may im-  
67 prove detection algorithms in addition to attribution algorithms by reducing the reliance of  
68 detection methods on perfect time series data and adherence of disturbance events to defined  
69 thresholds of change. However, most detection algorithms using computationally-intensive  
70 time series decomposition or modeling have not incorporated spatial data.

71       Recent advances in the availability of satellite remotely-sensed data have made increas-  
72 ingly innovative methods for detecting and attributing forest disturbances possible (Mc-  
73 Dowell et al. 2015, Curtis et al. 2018). For example, using dense time series of Landsat  
74 imagery, it is now possible to assess areas of forest loss and gain globally (Hansen et al. 2013,  
75 Tropek et al. 2014, Hansen et al. 2014). However, it remains a challenge to efficiently and  
76 accurately detect and attribute forest disturbances across varying disturbance severities and  
77 forest types. It is especially difficult to detect lower severity disturbances (Cohen et al. 2017,  
78 Curtis et al. 2018, Song et al. 2018). Several ensemble modeling methods have been proposed  
79 to improve disturbance detection accuracy across varying forest types and for lower severity  
80 disturbances. Ensemble approaches integrate results from multiple algorithms (Healey et al.  
81 2018), or multiple spectral bands or indices (Cohen et al. 2018). These approaches substan-  
82 tially decrease both commission (i.e., false positive) and omission (i.e., false negative) errors,  
83 but are computationally intensive as many iterations of detection must be completed before  
84 the secondary classification process.

85       Researchers are beginning to incorporate information on the spatial context of individual  
86 pixels (i.e., NPI) into attribution methods that make use of the temporal detection (i.e.,  
87 POI) approaches (Kennedy et al. 2015, Shimizu et al. 2017, Zhao et al. 2018); however, NPI  
88 may also be of use in the detection of forest disturbances. Disturbances do not occur in  
89 isolation, and therefore it is likely that if changes in the spectral band or index values are  
90 observed in a single pixel, neighboring pixels may also show similar changes (Gomez et al.  
91 2011). Thus, incorporating information on neighboring pixels into models of disturbance

presence or absence may substantially improve our abilities to find disturbances of lower severity or where time series data are incomplete or noisy due to the presence of clouds or snow. Additionally, the incorporation of NPI into the detection process enables a natural link of detection with attribution, making it possible to complete both processes using one analysis pipeline. For attribution, the characteristics of the neighboring pixels allow for differentiation between disturbance types because disturbances often vary considerably in their spatial signatures (Kennedy et al. 2015). For example, high severity fires may affect all pixels in an area similarly due to non-selective mortality or may impact all pixels within a short time frame. In contrast, a bark beetle outbreak might only affect some species in the area, leading to more patchy changes in spectral measures over the same area over a longer time period.

Machine learning has been applied to disturbance detection and attribution in several previous analyses, although primarily on either POI time series approaches (Huang et al. 2008, Lippitt et al. 2008, Rogan et al. 2008, Healey et al. 2018), or solely for attribution (Zhao et al. 2015, Shimizu et al. 2017). Using only POI spectral data, detection of partial forest harvest was up to 94% accurate in Massachusetts (Lippitt et al. 2008), and detection of varying large disturbances was 80% accurate in 19 Landsat scenes from around the world (Huang et al. 2008). While both of these approaches are promising, they were limited in their application by the training requirements and data preparation steps because high-quality, temporally-dense, Landsat data were not yet publicly available. More recently, machine learning has been applied to the attribution of forest disturbances. Attribution accuracies of 87% were achieved for wildfires, harvests, and other disturbances using Support Vector Machines in the Greater Yellowstone Ecosystem (Zhao et al. 2015), while attribution accuracies of harvests, water invasions, urbanization, other changes, and areas of recovery were 85 – 96% accurate using a Random Forest approach in the Bago Mountains, Myanmar (Shimizu et al. 2017). Combining both detection and attribution within a single analysis pipeline using machine learning could result in similarly high accuracies as previous studies,

119 while decreasing the amount of time and effort spent on the analysis.

120 Machine learning can also increase the transferability of detection and attribution algo-  
121 rithms, enabling regional- to global-scale analysis of disturbance type and regime. Distur-  
122 bances differ among ecosystems depending on myriad factors, including forest vegetation,  
123 climate, topography, and management (Sousa 1984). As a result, parameters of forest dis-  
124 turbances are not stationary and models that assume stationarity are limited in their scope  
125 (e.g., Fotheringham et al. 1996) meaning that current methods for detection are less suc-  
126 cessful when applied to ecological regions other than those for which they were developed  
127 (Cohen et al. 2017). Machine learning algorithms relax assumptions of stationarity of model  
128 parameters, and allow different models to be fit to different regions without potentially bi-  
129 ased user-specified parameters. Finally, approaches such as Random Forest allow for both  
130 the inclusion of numerous variables (i.e., POI and NPI) in detection and attribution models,  
131 and also quantify variable importance, providing valuable information about the typical tem-  
132 poral and spatial characteristics of disturbances among ecological regions. Understanding  
133 how disturbance characteristics vary spatially can inform further improvements to detection  
134 and attribution methods and enhance our understanding of spatially-varying disturbance  
135 impacts on ecosystem patterns and processes (Cooper et al. 2017).

136 Here, we introduce *disturbr*, a new approach for both the detection and attribution of  
137 disturbances in R. We apply *disturbr* to quantify and interpret patterns of disturbance char-  
138 acteristics across ecosystem types. In addition to using Random Forest models for both steps,  
139 we also incorporate spatial information on the area surrounding each POI. Our objectives  
140 with this new approach were to introduce and analyze the potential of spatial information  
141 and machine learning for disturbance detection and attribution, and to determine whether  
142 the *disturbr* approach improved the consistency of detection accuracies among multiple re-  
143 gions. We also sought to understand how disturbance characteristics differ across forest  
144 types, and how those differences might complicate traditional temporal approaches to dis-  
145 turbance detection.

<sup>146</sup> **2 Methods**

<sup>147</sup> Prepared Landsat imagery was summarized into variables representing both POI and  
<sup>148</sup> NPI variables over seven Landsat scenes across the United States. Training data for Random  
<sup>149</sup> Forest models were created through user observation of randomly-selected pixels over the  
<sup>150</sup> study scenes, and models were fit using POI and NPI variables. The final products of the  
<sup>151</sup> models were maps of disturbance locations and types, which were validated using out-of-bag  
<sup>152</sup> samples.

<sup>153</sup> **2.1 Scene selection**

<sup>154</sup> We chose the same study Landsat scenes (Fig. 1; Table 1) as those of previous disturbance  
<sup>155</sup> detection studies (Healey et al. 2018) so as to allow for more direct comparison of our results.  
<sup>156</sup> Collectively, these scenes represent a range of forest ecosystem and disturbance types to assess  
<sup>157</sup> the generality of the approach across regions. Scenes included a warm summer Mediterranean  
<sup>158</sup> mixed conifer forest in southwestern Oregon, a warm summer continental Mediterranean  
<sup>159</sup> spruce-fir forest in northern Colorado, a warm summer humid continental mixed pine forest  
<sup>160</sup> in northeastern Minnesota, a warm summer humid continental spruce-fir forest in western  
<sup>161</sup> Maine, humid subtropical mixed hardwood and pine forests in eastern Pennsylvania and New  
<sup>162</sup> Jersey, and a humid subtropical mixed hardwood and pine forest in eastern South Carolina  
<sup>163</sup> (Healey et al. 2018; Table 1). An additional Landsat scene was selected covering a temperate  
<sup>164</sup> rainforest/coastal mixed conifer forest in the Olympic Peninsula in Washington state, where  
<sup>165</sup> natural and anthropogenic disturbance types vary considerably (Peterson et al. 1997).

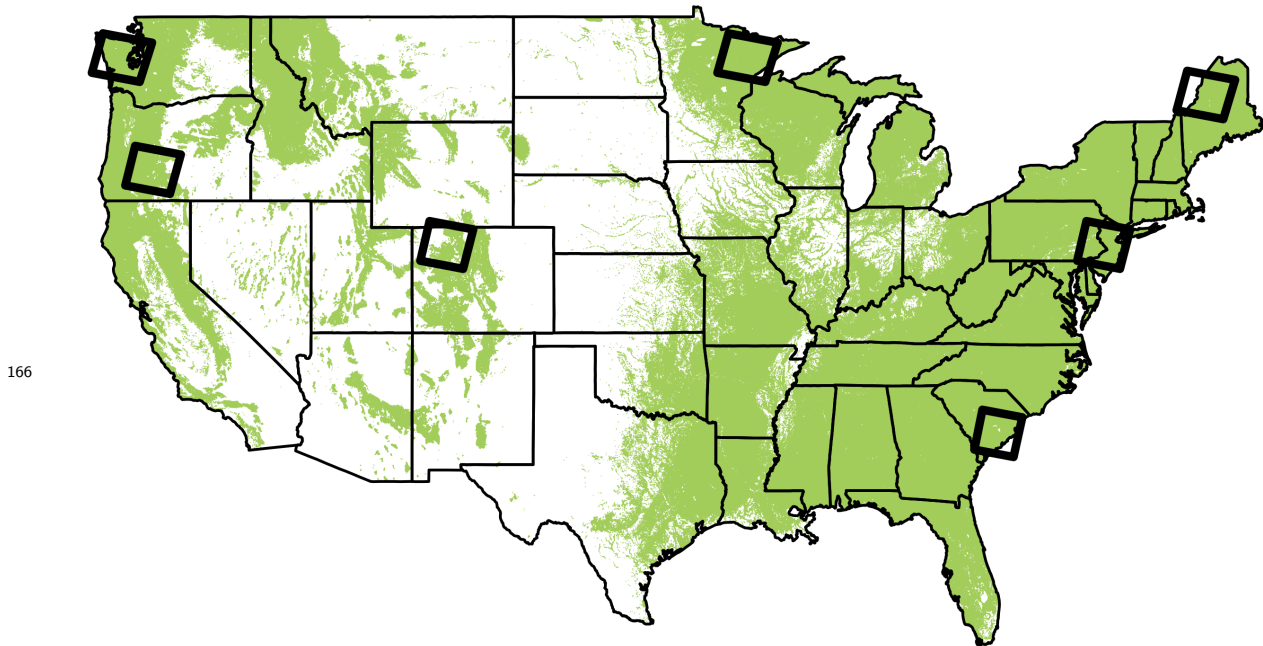


Figure 1: Location of Landsat scenes where *disturbr* was tested across the United States. Green areas show areas with  $\geq 20\%$  forest cover (Hansen et al. 2013).

## 167 2.2 Random Forest models for detection and attribution

168 For each scene, we applied separate Random Forest models for both the detection and at-  
 169 tribution components of *disturbr* because they have proven to be effective in past disturbance  
 170 detection and attribution approaches (Lippitt et al. 2008, Kennedy et al. 2015, Schroeder  
 171 et al. 2017, Cohen et al. 2018, Healey et al. 2018). Random Forests are randomized decision  
 172 trees, which may be less prone to model overfitting than ordinary decision tree methods  
 173 (Breiman 2001, Pal and Mather 2003). Random Forests take multiple random subsets of the  
 174 complete training dataset and create decision trees with each subset. When data are run  
 175 through the model (i.e., set of decision trees), the result (disturbance class) with the most  
 176 votes from all trees is the predicted class.

Table 1: Landsat scenes included in the study and the primary disturbance types present in each scene.

Region Name	Landsat Path	Landsat Row	Primary Disturbance Types
Washington (WA)	47	27	Harvest, River Changes, Development
Oregon (OR)	45	30	Fire, Harvest
Colorado (CO)	35	32	Fire, Bark Beetle Outbreaks
Minnesota (MN)	27	27	Harvest, Flooding, Development
Maine (ME)	12	28	Harvest
South Carolina (SC)	16	37	Harvest, Development
Pennsylvania/New Jersey (PA)	14	32	Development

### 2.3 Data preparation

For each Landsat scene (Table 1), we prepared NDVI data for seven scenes across seventeen years in Google Earth Engine (Gorelick et al. 2017) using both Tier 1 Landsat 5 and Landsat 7 top-of-atmosphere (TOA) images (Chander et al. 2009). Areas with clouds, shadows, water, and snow were removed from all tiles from the study period (2000 – 2016) using the information in the QA band, derived using CFMask. The Tier 1 TOA data are the highest quality Landsat images available, and may be considered radiometrically calibrated and geolocated consistently ([landsat.usgs.gov](http://landsat.usgs.gov)). Summertime mean (June-July-August) NDVI was calculated using all available annual imagery over the study period and each region. If both Landsat 5 and 7 imagery were available, all TOA images from both satellites were used in calculating the mean.

Forty-seven variables were created in R as potential predictors for the disturbance detection model (Fig. 2). Variables were created based on observed differences between disturbed and undisturbed pixels, including known metrics for identifying disturbance (e.g., magni-

<sup>192</sup> tude and duration drop in greenness). The large number of variables allowed us to better  
<sup>193</sup> describe the ecological complexity of disturbed and undisturbed forests across a wide range  
<sup>194</sup> of systems.

<sup>195</sup> POI variables were calculated using 2000 – 2016 NDVI time series for a single pixel,  
<sup>196</sup> and NPI variables were calculated using time series for the nearest 64 pixels (including the  
<sup>197</sup> POI), or roughly a circular region within a 270m x 270m window around the POI (Fig.  
<sup>198</sup> 2B). NDVI was selected for this analysis due to its widespread use in previous studies (e.g.,  
<sup>199</sup> Mildrexler et al. 2007, Verbesselt et al. 2012) and its relative simplicity to calculate. POI  
<sup>200</sup> predictor variables were produced using several models fit to the time series, including a  
<sup>201</sup> simple smoother (loess), a simple linear model (R Core Team 2017), and a regression tree  
<sup>202</sup> (Therneau et al. 2017). These variables provided different information on breaks in the time  
<sup>203</sup> series, overall trend, locations of maxima and minima, and trend in NDVI recovery if a  
<sup>204</sup> negative break in the time series (NDVI decline) occurred. Additional variables provided  
<sup>205</sup> information on overall time series characteristics such as pre- and post-disturbance variation  
<sup>206</sup> (Fig. 2).

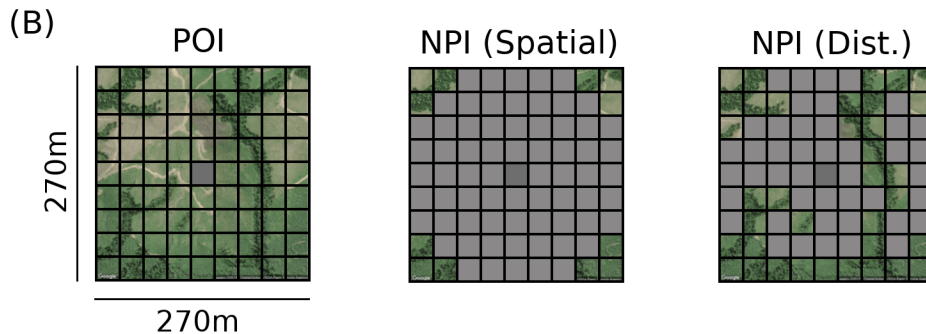
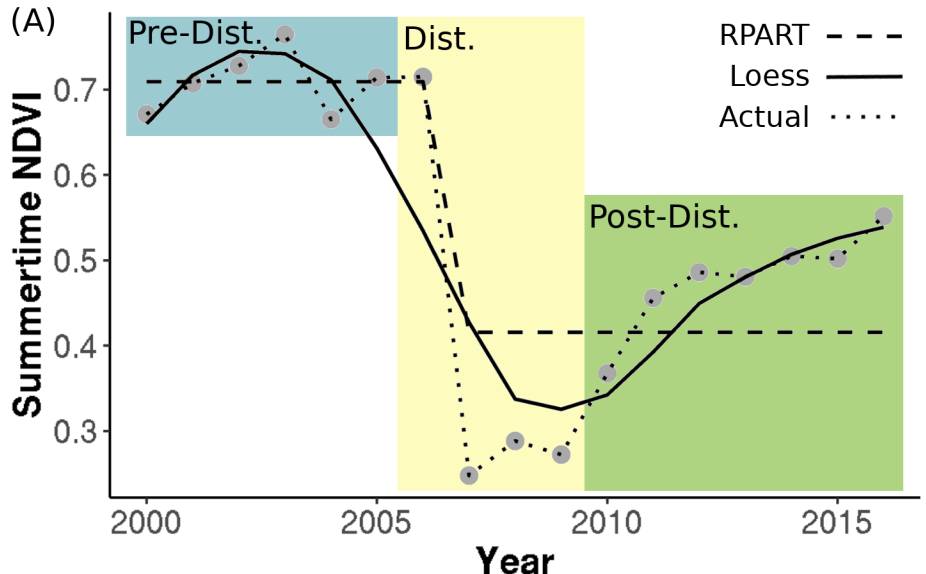


Figure 2: (A) NDVI time series for a harvest disturbance in Washington. Pixel-level variables representing time series components (e.g., minimum slope, variance) were calculated using either the raw time series, indicated by the points and dotted line, the fitted loess curve, indicated by the plain line, or the fitted curve from an RPART model, indicated by the dashed line. A full variable list is shown in Fig. S3. (B) Domains of model predictor variables. Gray pixels represent the pixels over which variables were calculated for the POI, and the nearest 64 pixels (NPI). The NPI (Dist.) grid indicates predicted disturbance pixels over the area.

208 **2.4 Detection modeling**

209 We developed training methods in R for the Random Forest detection models with a  
 210 sequence of steps. First, each Landsat scene was split into 9 blocks to reduce computational  
 211 requirements. Second, we randomly selected 200 pixels from each of three blocks along the  
 212 diagonal of the scene (top-left to bottom-right), resulting in 600 potential training points  
 213 for each scene. The disturbance state for some pixels could not be determined, so the final

number of training points for each scene was  $507 \pm 89$  pixels. Third, for each pixel in the sample, we determined the presence or absence of a disturbance, and the type of disturbance if present, based on a time series of NDVI images for the area surrounding the pixel, a recent true-color satellite image (via Google Earth; Google 2019), and a line plot of NDVI over the study period plotted with a loess curve (an approach similar to TimeSync; Cohen et al. 2010). Our streamlined method in R minimizes the number of programs required by *disturbr* users by removing the need to move data to and from separate programs. TimeSync (Cohen et al. 2010), the approach on which this training method was based, has been widely applied to similar analyses (Masek et al. 2013, Zhao et al. 2015, Cohen et al. 2018). This approach to creating training data enables researchers to train data anywhere with available remote sensing time series. Following training, we fit a Random Forest model with the ‘rf’ function (Liaw et al. 2002) in the ‘caret’ package in R (Kuhn 2015), with all 47 variables. The resulting detection model was used to produce a preliminary classification of either disturbed or undisturbed for all pixels within each Landsat scene.

## 2.5 Attribution data preparation

Seventeen additional spatial variables describing the characteristics of a disturbance over the neighboring pixels were created using the detection results, to provide supplementary information for the attribution models. These variables relied on pixels which had been marked as disturbed by the initial model, and describe the similarity in disturbance characteristics of the 64 nearest neighboring pixels (including the POI) (Fig. 2). For example, many of these variables describe the mean or range, magnitude, duration, or other time series characteristics for disturbed pixels within neighboring areas.

## 2.6 Attribution modeling

We prepared training data for the attribution model using the same method as described for the detection models (section 2.4). We first assessed which of the detection training points overlapped with predicted disturbance locations. Those pixels were then combined

240 with additional training data from a random sample of 50 new pixels for each training  
241 block. With some of the pixels removed because the disturbance could not be identified,  
242 this resulted in a total of  $166 \pm 41$  attribution training points for each scene. When unsure  
243 of the disturbance type during training, we checked the point using historical imagery in  
244 Google Earth Pro (Google 2019). While this additional check was time-intensive, it was not  
245 required very frequently. We also assessed false positives during this process by including  
246 false positive as a potential disturbance class. A false positive was indicated if the pixel  
247 was labeled as disturbed by the detection model, but was identified as undisturbed in the  
248 50 new training pixels during the attribution training step. Disturbance types included in  
249 the training were biotic disturbances (e.g., bark beetles or defoliators), fire, harvest, wind,  
250 water (e.g., flooding or changes in river path), development (e.g., construction or mining),  
251 and landslides and avalanches. These categories were user-defined and are therefore flexible  
252 for studies with varying objectives.

253 The Random Forest model to attribute the previously-detected potential disturbance  
254 locations was fit using the same method as the detection model. The resulting model was  
255 used to attribute predicted disturbances to individual disturbance classes or remove them  
256 as false positives. Output from this final step included a map of disturbance locations and  
257 types, as well as a map of disturbance year (Fig. 3). To determine the predicted disturbance  
258 start year, first we fit a loess smoother to the raw NDVI time series for each pixel. Then  
259 we determined the minimum slope over the smoothed time series (considering all possible  
260 slopes). The disturbance start year was the year which corresponded to the start of the  
261 minimum slope segment of the smoothed time series (Fig. 2).

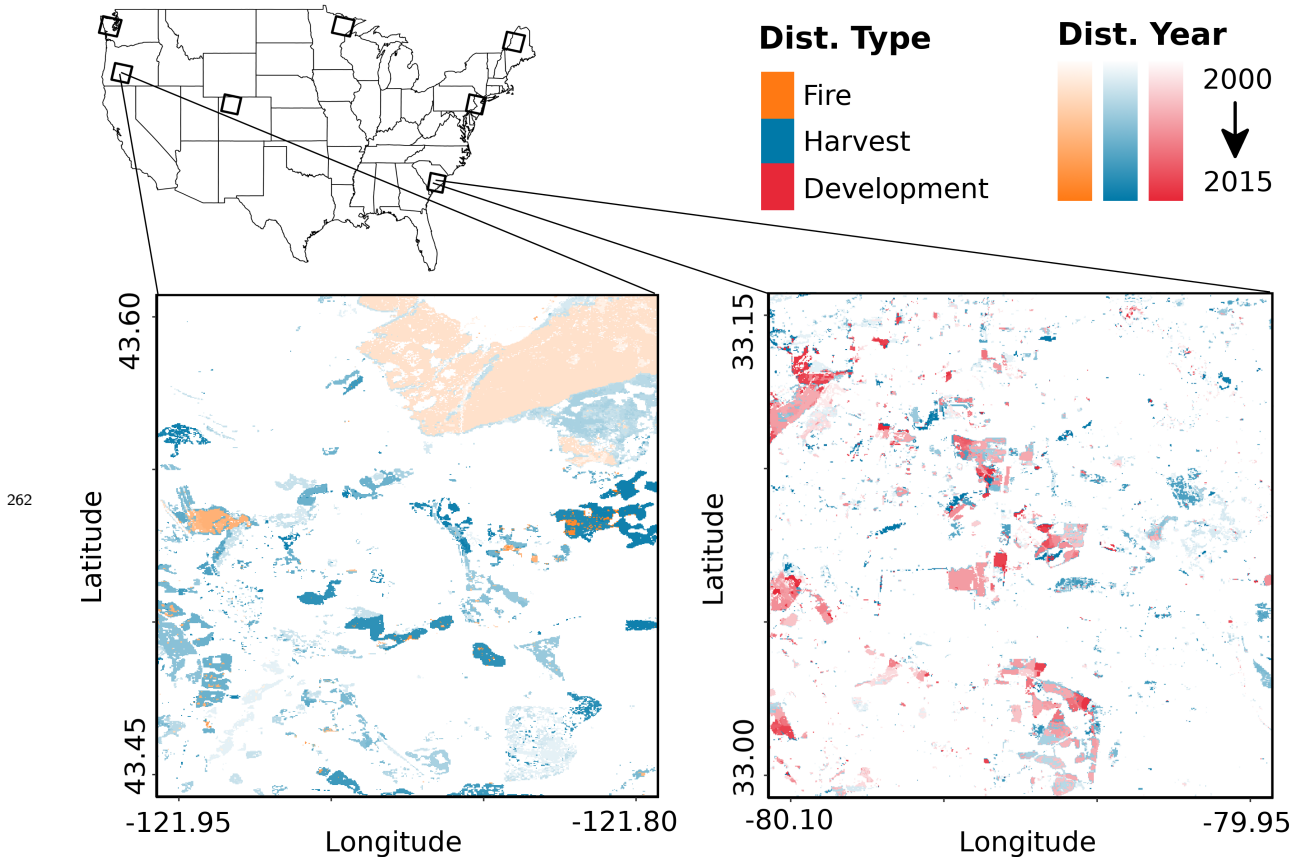


Figure 3: Detection and attribution results from *disturbr* for portions of Oregon and South Carolina. The large 2003 Davis Lake fire and nearby harvest are clearly visible in Oregon, while steady development and harvest are prominent in South Carolina.

## 263 2.7 Validation

264 We used historical satellite imagery in Google Earth Pro (Google 2019) to validate the  
265 model predictions of disturbance locations and types. First, we determined whether a disturbance  
266 had actually occurred in the labeled points and whether no disturbance was present  
267 in the unlabeled points using out-of-bag samples. We checked pixel labels using both his-  
268 torical satellite imagery in Google Earth Pro, and the training methods described in section  
269 2.4. Validation for disturbed and undisturbed locations was completed for three randomly-  
270 selected blocks within each Landsat scene, with 100 pixels selected from each block. The 100  
271 random pixels from each block yielded a sample of both disturbed and undisturbed pixels,  
272 with sample numbers proportional to the disturbed/undisturbed ratio for each scene. How-

273 ever, in several cases the proportion of disturbed pixels was very small (i.e., 1 or 2 pixels).  
274 Therefore, we increased the disturbed pixel sample number to 50 if it fell below that value.  
275 This resulted in a total validation sample of  $384 \pm 32$  pixels per scene. Validation pixels  
276 overlapping with training points were removed from the validation set. Accuracy metrics  
277 calculated included raw commission and omission errors in addition to Cohens kappa statistic  
278 (Cohen 1968) for overall accuracy.

279 Second, we determined the attribution accuracy. While validating whether or not a pixel  
280 labeled disturbance was disturbed, we also noted the actual type of disturbance present. We  
281 then determined the percentage of pixels within each block and scene that were both labeled  
282 disturbed and had the correct disturbance type label.

283 Third, we assessed the accuracy of the predicted disturbance date from the model by  
284 comparing the predicted starting year of disturbance with the observed year at which the  
285 disturbance event began. The observed disturbance start year was determined using the raw  
286 time series and locating the year prior to the disturbance-induced NDVI decline.

## 287 **2.8 Variable importance**

288 Variable importance for both detection and attribution models was assessed using the  
289 ‘varImp’ function in the ‘caret’ R package (Kuhn 2015). Variables were ordered by their  
290 Gini importance and the top five most important variables were assessed more closely to  
291 determine which variables and types of variables showed up most frequently as being of  
292 highest importance to the models. We also tested the value of including NPI variables in  
293 the detection model by assessing the difference in the number of pixels labeled disturbed in  
294 addition to the overall detection accuracy of models fit with and without NPI variables.

## 295 **3 Results**

### 296 **3.1 Detection accuracy**

297 The overall kappa detection accuracy for each scene ranged between 67% (SC — path  
298 16, row 37) and 88% (PA/NJ — path 14, row 32), with a median kappa accuracy of 76%.

<sup>299</sup> Commission rates were  $16 \pm 6\%$ , and omission rates were  $8 \pm 6\%$  (Table 2; Fig. S1). The  
<sup>300</sup> highest commission rates (25%) occurred in Maine. South Carolina had the highest omis-  
<sup>301</sup> sion rates (19%) (Table 2; Fig. S1). Within each scene, *disturbr* accuracy also varied among  
<sup>302</sup> validation blocks (Table 2). The highest variation in both commission and omission rates  
<sup>303</sup> among validation blocks occurred in Colorado (commission  $\sigma^2 = 54\%$ ; omission  $\sigma^2 = 30\%$ ),  
<sup>304</sup> and commission and omission rates were the most consistent among blocks in Pennsylva-  
<sup>305</sup> nia/New Jersey (commission  $\sigma^2 = 3\%$ ; omission  $\sigma^2 = 1\%$ ). The high standard deviation  
<sup>306</sup> among blocks in Colorado was due to the inclusion of a block containing very few forested  
<sup>307</sup> pixels, including only 3 pixels labeled disturbance (Fig. S1).

Table 2: Commission and omission rates, and kappa accuracy values for each Landsat scene.

Region	Validation Name	Commission Block	Omission Rate (%)	Kappa Accuracy (%)	<i>n</i> Disturbed	<i>n</i> Undisturbed
WA	2	4.00	7.25	88.03	50	69
	3	29.17	6.85	66.11	48	73
	6	34.69	3.85	64.91	49	78
	<i>all</i>	22.45	5.91	73.30	147	220
OR	1	26.32	0	79.22	38	81
	4	5.26	3.53	90.55	38	85
	5	9.52	2.27	89.32	42	88
	<i>all</i>	13.56	1.97	86.63	118	254
CO	2	13.33	6.74	79.93	45	89
	7	100	0	0	3	100
	9	0	55.10	47.65	62	49
	<i>all</i>	8.18	13.87	73.63	110	238
308 MN	1	25.81	4.04	73.41	31	99
	4	15.91	10.20	75.52	44	98
	6	13.95	8.51	76.57	43	94
	<i>all</i>	17.80	7.56	74.46	118	291
ME	2	17.65	13.48	65.31	34	89
	3	14.29	9.89	73.25	35	91
	7	46.67	0	63.41	30	94
	<i>all</i>	25.25	7.66	67.96	99	274
SC	1	10.42	18.18	68.97	48	77
	4	4.54	23.08	67.06	44	78
	5	22.00	14.29	63.71	50	77
	<i>all</i>	12.68	18.53	66.52	142	232
PA/NJ	1	16.00	1.02	85.93	50	98
	7	14.29	2.00	85.95	49	100
	8	10.20	1.01	90.65	49	99
	<i>all</i>	13.51	1.34	87.51	148	297

### 309 3.2 Attribution accuracy

310 Incorrect attribution to disturbance type occurred at rates of  $18 \pm 10\%$  (Fig. 4), with the  
 311 highest rate in Minnesota, and the lowest rate in Pennsylvania/New Jersey (Fig. 4). High  
 312 rates of incorrect attribution to disturbance type occurred in areas with more disturbance  
 313 types, or in areas with rare disturbances that were not caught in the training data. For

example, both Washington and Oregon had relatively high rates of incorrect attribution, and  
 also had more than three disturbance types present. Pennsylvania/New Jersey and South  
 Carolina had relatively low rates of incorrect attribution, and only a couple of common  
 disturbance classes. On the other hand, a rare large bog fire in Minnesota was missed in  
 training, resulting in high rates of misclassification due to the fire being classified as harvest  
 (Fig. 4). Attribution accuracy also varied among blocks, with Minnesota having the least  
 consistent attribution accuracy ( $\sigma^2 = 35\%$ ) due to the misattribution of the fire and Colorado  
 having the most consistent attribution accuracy ( $\sigma^2 = 6\%$ ).

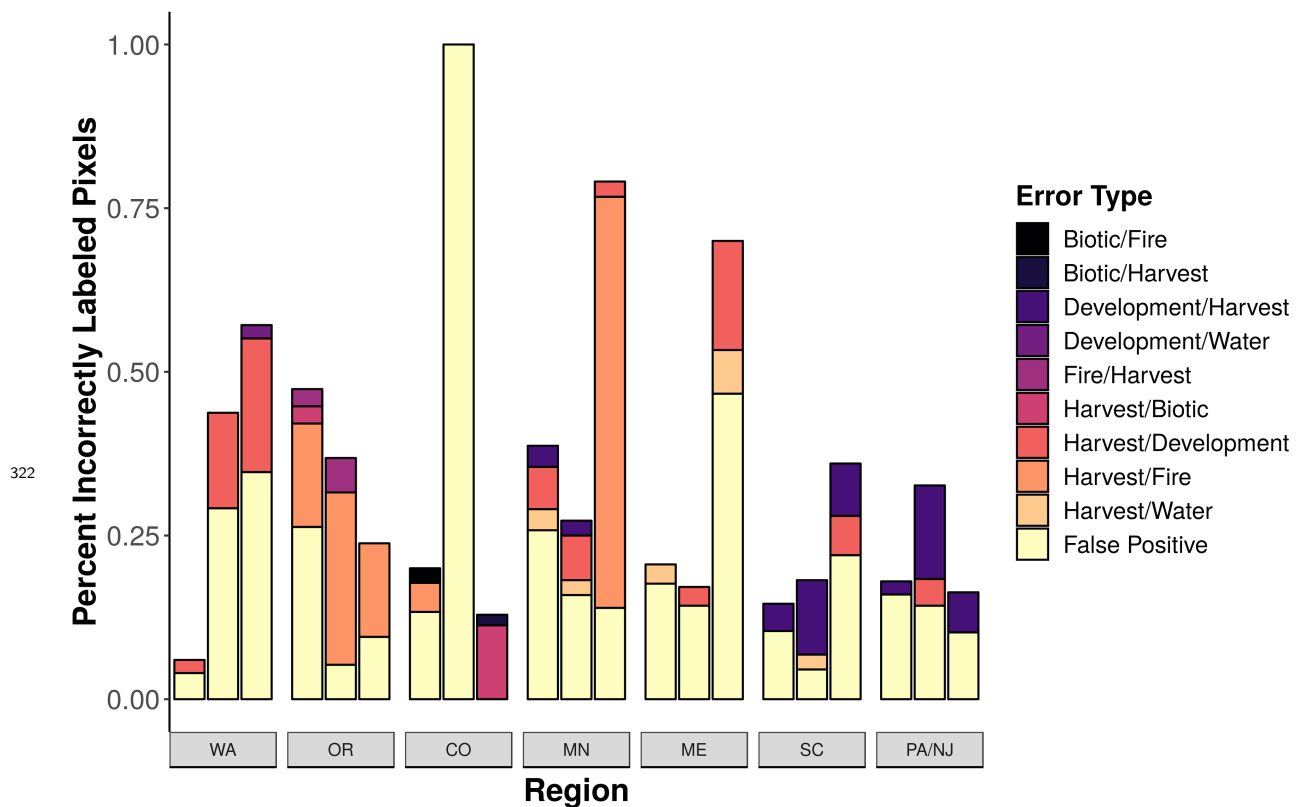
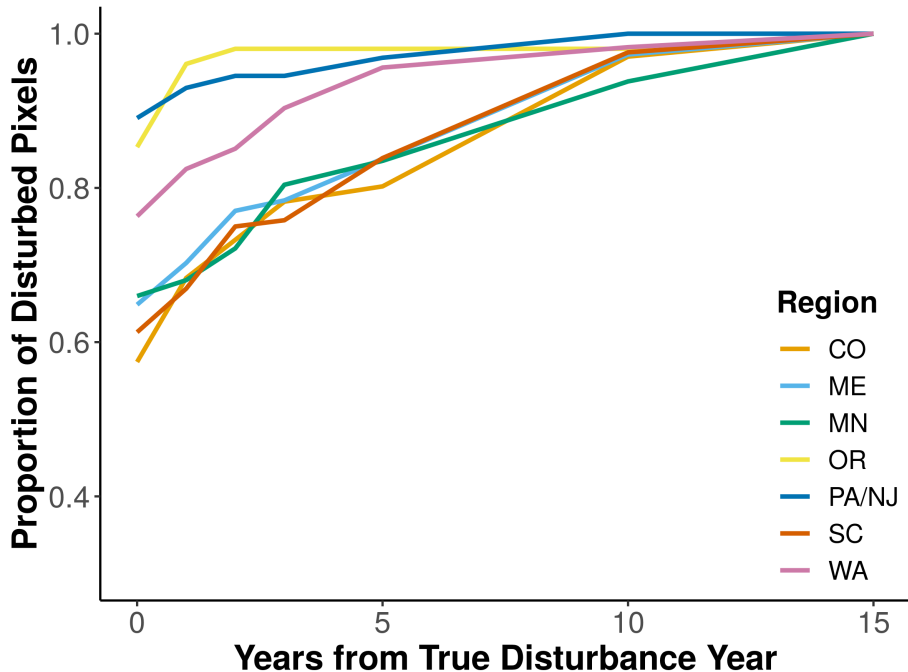


Figure 4: Types of errors in pixels labeled disturbance for each validation block within each Landsat scene. The bars for each region correspond to the order of validation blocks in Table 2. Error types are formatted as labeled disturbance type/actual disturbance type. Actual pixel numbers are shown in Fig. S2.

### 3.3 Disturbance year accuracy

The year of disturbance was identified correctly in 57 – 89% ( $\mu = 71\%$ ) of the correctly-  
 identified disturbances, with 76 – 95% ( $\mu = 85\%$ ) of disturbances dated to within 3 years

326 of the true disturbance date (Fig. 5). The lowest accuracy rate for disturbance year was  
 327 in Colorado (57%), while the highest accuracy rate for disturbance year was in Pennsylva-  
 328 nia/New Jersey (89%). Incorrect identification of disturbance year was more common for  
 329 gradual or lower-severity disturbance events such as insect outbreaks. Rates for the correct  
 330 identification of year of disturbance also varied slightly among blocks, although accuracy  
 331 rates of blocks used for training were not any different than those of blocks not used for  
 332 training.



333  
 334 Figure 5: Accuracy of the predicted disturbance date. The y-axis indicates the proportion of disturbed  
 335 pixels in each scene, indicated by different colors, which were identified within a certain distance from the  
 336 true disturbance year (on the x-axis).

### 337 3.4 Variation in disturbance characteristics among ecosystems

338 The importance of variables in the models for predicting disturbance presence/absence  
 339 and type varied among regions (Table 3). For instance, while the overall drop in the time  
 340 series (i.e., disturbance magnitude) was important for distinguishing disturbed areas from  
 341 undisturbed areas in Washington (Fig. 6, Table 3, Fig. S4), the overall time series variance  
 342 was much more important in Pennsylvania/New Jersey (Table 3; Fig. S4). While the impor-

<sup>340</sup> tant variables differed by region, several types of variables did show consistent importance  
<sup>341</sup> as well (Table 3). Information on the minimum slope of the time series was consistently  
<sup>342</sup> important for both detection and attribution, as was the variance of the time series.

<sup>343</sup> Overall, temporal variables held more importance for determining the presence of dis-  
<sup>344</sup> turbances, while spatial variables gained importance for classifying the type of disturbance.  
<sup>345</sup> Four out of seven scenes included spatial variables in the top five most important for de-  
<sup>346</sup> tection, while all seven scenes included spatial variables in the top five most important for  
<sup>347</sup> attribution (Table 3). We tested the value of spatial information to disturbance detection by  
<sup>348</sup> running the detection models both with and without spatial variables. The detection results  
<sup>349</sup> differed by  $3 \pm 3\%$  in terms of numbers of pixels labeled disturbed, while the accuracy of  
<sup>350</sup> the detection models alone differed by 2 – 21% between the models with and without spatial  
<sup>351</sup> information (Table S1; kappa accuracy with spatial:  $76 \pm 8\%$ ; without spatial:  $69 \pm 11\%$ ).  
<sup>352</sup> The largest improvement due to the incorporation of spatial variables, 21%, occurred in Col-  
<sup>353</sup> orado where the primary disturbance type was bark beetle-induced mortality. This indicates  
<sup>354</sup> that spatial information has the potential to improve detection results for low severity and  
<sup>355</sup> spatially heterogeneous disturbance types.

<sup>356</sup> The most important predictor variables for detection were the variance in the loess slope  
<sup>357</sup> of the time series, as well as the minimum loess slope (Table 3, Fig. 2). The most important  
<sup>358</sup> predictor variables for attribution were the spatial range in minimum loess slope for all  
<sup>359</sup> neighboring pixels and only disturbed pixels, the spatial average of minimum loess slope,  
<sup>360</sup> and the spatial range of pixel-level mean NDVI for disturbed pixels. Overall, the loess slope  
<sup>361</sup> variables tended to be much more important than the regression tree or raw time series  
<sup>362</sup> slope variables, although some of those variables were among the top five most important  
<sup>363</sup> variables in several models. Overall, disturbance timing (e.g., range in dates over the area)  
<sup>364</sup> and duration were not especially important in the models.

Table 3: Top five most important variables for the Random Forest detection and attribution models of each Landsat scene. Light gray shading indicates variables that were summarized over the nearest 64 pixels surrounding the POI (including the POI); dark gray shading indicates variables that were summarized over pixels labeled disturbed within the nearest 64 pixels surrounding the POI (including the POI). All other variables are representative of the POI only. Statistics in parentheses (e.g., (Mean)) indicate the summary statistic over the larger area for spatial variables.

Region	Detection Variables		Attribution Variables
WA	Min. Loess Slope		Max. NDVI
	Var. Loess Slope		Min. Slope
	Range Loess Curve		Min. Loess Slope (Mean)
	Magnitude		Mean NDVI (Range)
	Min. Loess Slope (Mean)		Mean NDVI (Median)
OR	Loess Slope		Min. NDVI
	Min. Reg. Tree Slope		Min. Loess Slope (Mean)
	Min. Loess Slope		Min. Loess Slope (Range)
	Var. Loess Slope		Max. Loess Slope (Ratio)
	Post-Dist. Var.		Min. Loess Slope (Range)
CO 365	Loess Slope		Var. Slope
	Min. Loess Slope		Min. Loess Slope (Mean)
	Var. Loess Slope		Min. Loess Slope (Range)
	Pre-/Post-Dist. Var. Ratio (Mean)		Min. Loess Slope (Range)
	Magnitude (Mean)		Min. Loess Slope (Median)
MN	Variance		Min. NDVI
	NDVI Range		Mean Avg. Deviance/Mean Ratio
	Var. Slope		Magnitude
	Var. Loess Slope		Min. Loess Slope (Ratio)
	Min. Loess Slope (Mean)		Mean NDVI (Range)
ME	Variance		Mean Slope
	Mean Avg. Deviance		Min. Loess Slope (Mean)
	Max. Loess Slope		Min. Loess Slope (Range)
	Var. Loess Slope		Mean NDVI (Range)
	Range Loess Curve		Mean NDVI (Median)
SC	Min. NDVI		Mean NDVI
	Min. Loess Slope		Loess Slope
	Var. Loess Slope		Mean Loess Slope
	Post-Dist. Var.		Min. Loess Slope (Range)
	Min. Loess Slope (Range)		Min. Loess Slope (Range)
PA	Min. Loess Slope		Loess Slope
	Var. Loess Slope		Min. Loess Slope (Range)
	Range Loess Curve		Mean NDVI (Range)
	Pre-/Post-Dist. Var. Ratio		Loess Slope (Range)
	Magnitude		Min. Loess Slope (Median)

366 **4 Discussion**

367 We present a streamlined and transferrable detection and attribution technique, *disturbr*,  
368 capable of both accurately locating and characterizing disturbances across a range of ecosys-  
369 tems. This new approach fills a critical methodological gap in the movement towards high  
370 resolution disturbance mapping — the flexibility for methods to be applied around the globe  
371 with disturbance definitions tuned to local conditions (Tropek et al. 2014). Specifically, the  
372 approach has several advantages: it uses spatial information to detect and attribute forest  
373 disturbance, it enables attribution of specific disturbance types, and it is transferable across  
374 multiple ecoregions.

375 **4.1 Incorporating spatial information and machine learning for disturbance de-**  
376 **tetection and attribution**

377 For our first objective, we successfully developed a novel detection and attribution ap-  
378 proach, incorporating NPI through the use of machine learning models, with accuracy results  
379 comparable to forest disturbance detection results from strictly POI detection approaches.  
380 As with other studies (e.g., Zhu et al. 2012, Cohen et al. 2018, Healey et al. 2018), *disturbr*  
381 resulted in higher accuracies for large or severe disturbances (e.g., clearcut harvests) when  
382 compared to smaller or less severe disturbances (e.g., beetle-kill or small-scale construction).  
383 Additionally, while our labeled detection year was close to the true disturbance year for  
384 larger or more severe disturbances, that accuracy declined as disturbances became smaller,  
385 more spatially distributed, and less severe. However, we did show that models incorporating  
386 spatial variables can improve detection results when applied in areas with smaller or lower  
387 severity disturbances. Importantly, *disturbr* achieved high accuracy rates with a commonly-  
388 used and open source platform (R) and was successful in detecting many differing types of  
389 disturbances in multiple locations. The method also allows users to detect and attribute  
390 disturbances in a single platform rather than having to use different approaches and plat-  
391 forms for each step. A final benefit comes from the flexibility of *disturbr* to use alternative

392 data sources, which enables it to be used in unique ways by each potential user (e.g., with  
393 alternative satellite indices).

394 To our knowledge, *disturbr* is the first method to use spatial information (i.e., NPI) for  
395 both the detection and attribution of forest disturbances. Incorporating spatial terms allows  
396 users to make use of more incomplete datasets and may therefore be useful in areas of the  
397 world with less complete collections of satellite imagery. Additionally, the incorporation of  
398 NPI into disturbance detection allows for more clear-cut differentiation of data abnormalities  
399 from true disturbances, as forest disturbances tend to have fairly distinct spatial character-  
400 istics (Foster et al. 2003, McIntire and Fajardo 2009). Specifically, the incorporation of NPI  
401 is useful for removing false detections related to our use of Landsat 7 during the years in  
402 which the scan line corrector failed without having to exert substantial efforts in correcting  
403 the errors. While these areas were occasionally labeled using our detection model, composed  
404 of primarily POI variables, they were easy to remove (i.e., mark as false positives) in the  
405 secondary attribution step, which was completed using models incorporating more NPI vari-  
406 ables. Finally, despite the detection models being composed of mostly POI variables, we  
407 showed that NPI variables played a significant role in those models. The incorporation of  
408 NPI variables improved detection model accuracies by between 2 and 21%, with the most  
409 dramatic improvement in accuracy occurring in Colorado where the primary disturbance  
410 type, insect damage, is typically lower in severity. Therefore, the inclusion of NPI into  
411 disturbance detection has the potential to improve our ability to accurately and efficiently  
412 detect disturbances across a wide variety of forest types around the globe.

413 In addition to incorporating NPI to detection and attribution models, we also used a  
414 machine learning approach, Random Forests (Breiman 2001), to classify pixels into disturbed  
415 and undisturbed categories, and then into different disturbance types. While several studies  
416 have made use of Random Forests for the attribution component of this process, Random  
417 Forests have not been applied to detection. We believe that this application of Random  
418 Forests simplifies and improves the detection component by limiting reliance on perfectly

419 processed time series data. Rather than looking at the time series as a whole, the model uses  
420 general characteristics of the series, such as overall variance and minimum slope, to create  
421 more complex rules for what disturbed pixels look like relative to undisturbed pixels. The use  
422 of regionally-specific training data also improves the classification process, by allowing forests  
423 to have different characteristics. The use of many variables in combination with localized  
424 training allows the algorithm to incorporate these characteristics, and may therefore be more  
425 robust in the face of variable climate and differing forest ages among regions.

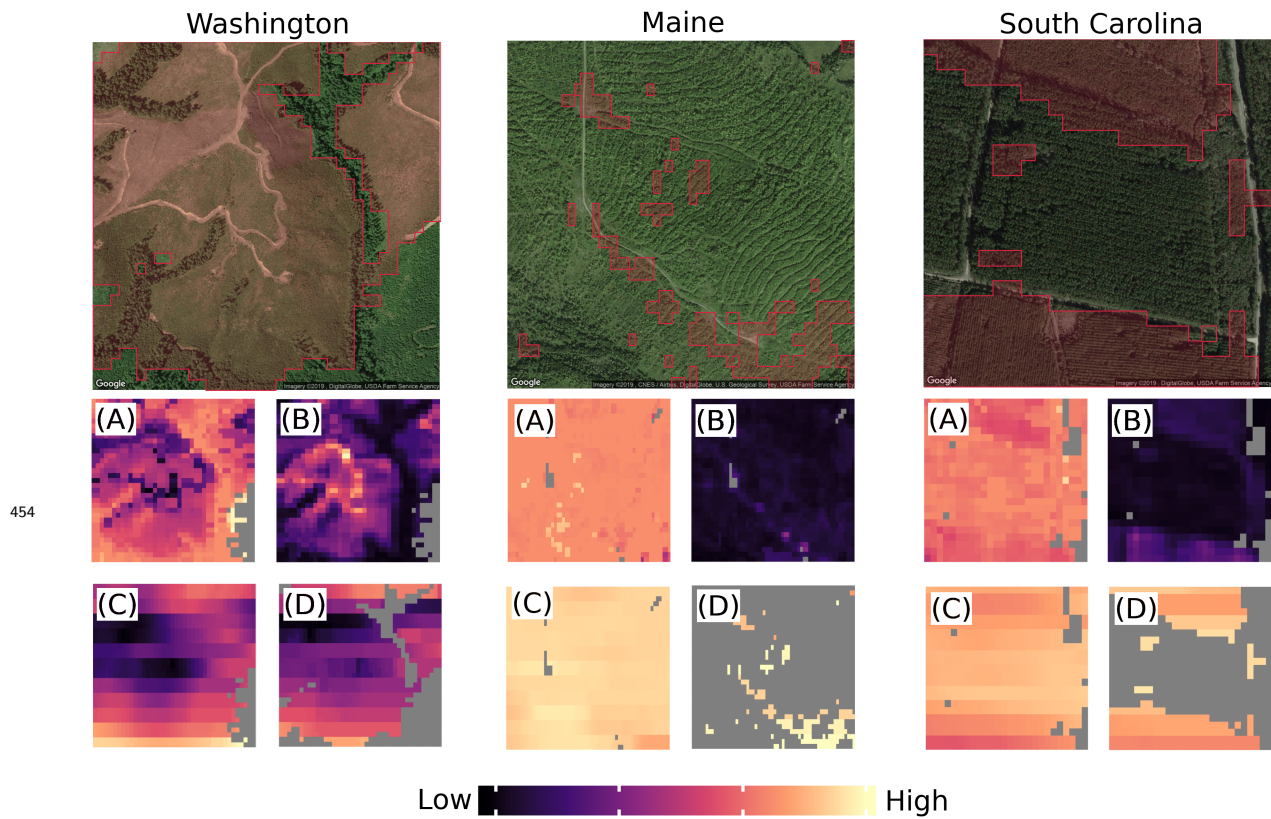
## 426 **4.2 Consistency of detection and attribution results across multiple regions**

427 Our second objective was to improve on the transferability of detection and attribution  
428 approaches. Cohen et al. (2017) found that detection algorithms are less successful when  
429 applied to regions in which they were not developed. Our accuracy results were relatively  
430 consistent across differing Landsat scenes and therefore ecosystems and forest types (Table  
431 2; Fig. S2). However, there was still substantial variability in the exact commission and  
432 omission errors within individual sites, especially across management zones or land use classes  
433 (Table 2). This variation is likely a result of the differing types of disturbances and forest  
434 characteristics that exist within Landsat scenes. Some areas have a higher percentage of  
435 larger and more severe disturbance events relative to others, or different types of disturbance  
436 altogether. While we can improve our ability to detect all types of disturbances, including  
437 smaller and less severe disturbances such as insect outbreaks, it is unlikely that any method  
438 will achieve perfect symmetry in accuracies among differing areas due to the inherent spatial  
439 differences in ecosystem and disturbance characteristics.

## 440 **4.3 Differences in disturbance characteristics among ecosystems and forest types**

441 Our third objective was to determine differences in disturbed and undisturbed forest  
442 characteristics, and how those characteristics influence detection and attribution method  
443 transferability. The variables included in the detection and attribution models for this anal-  
444 ysis are representative of several disturbance characteristics (e.g., disturbance severity, dura-

445 tion) (Fig. 6). As such, the variation in variable importance also provides information about  
 446 why disturbance detection methods may be less successful when transferred from regions in  
 447 which they were developed to new regions. With *disturbr*, we found variation in both undis-  
 448 turbed and disturbed forest characteristics among regions (Table 3; Fig. S4). The presence  
 449 of differences between forest types and disturbance regimes likely account for the reduced  
 450 ability of disturbance detection approaches based solely on POI time series characteristics to  
 451 transfer among different regions without substantial re-tuning. With *disturbr*, training data  
 452 are created for each ecological domain, thus minimizing biases in detection and attribution  
 453 among ecosystem types.



454  
 455 Figure 6: Examples of timber harvest results from Washington (path 47, row 27), Maine (path 12, row 28), and South Carolina (path 16, row 37). The top panels show the most recent Google satellite image  
 (Google n.d.) of the disturbed area, with the pink overlay showing areas that were labeled as disturbed  
 using *disturbr*. The bottom panels show the (A) magnitude, (B) variance, (C) spatial mean of magnitude,  
 and (D) disturbance spatial median of magnitude over the area. Gray areas indicate NA values.

The variation in disturbance detection ability may also vary by region because climate,

456 land use, and land cover mediate the measurable effects of different disturbances (Cooper  
457 et al. 2017). We found that lower accuracies resulted from more overlap among classes (e.g.,  
458 disturbed vs. undisturbed, or fire vs. insect damage) in the value distributions of variables.  
459 This may occur in areas with strong variation in forest conditions (e.g., climatic conditions),  
460 in areas with many types of forests or management scenarios (Niemelä 1999), or in regions  
461 with very low severity or small disturbances where disturbance states are mixed within small  
462 areas (e.g., following insect damage).

#### 463 4.4 Potential applications

464 Currently, *disturbr* is most useful at the local to regional scale (i.e., ecoregions and  
465 smaller) because creating a training dataset as large as that used in this analysis takes a  
466 considerable amount of time. At local to regional scales, users may relatively quickly train  
467 points for their study region (see section 2.4) and produce accurate detection and attribution  
468 results. The analysis presented here was completed with the High Performance Computing  
469 cluster at Michigan State University. A single Landsat scene took 2 – 5 days of computing  
470 time with 1 node, 9 cores, and between 40 and 120G memory depending on the step and  
471 Landsat scene; the entire analysis (excluding training) for this study was completed in ~1  
472 week as all scenes were run in parallel as separate jobs. An initial test run of *disturbr* with  
473 coarser resolution data (90m) on a single desktop machine with 32G memory and 12 cores  
474 took <1 week to process a single Landsat scene. The computational requirements for the  
475 *disturbr* framework are still quite high, but there are several ways in which it may be sped  
476 up in the future, including converting many of the R functions to C and incorporating the  
477 ability to train the models with polygon data (e.g., from aerial detection surveys or the  
478 Monitoring Trends in Burn Severity database).

479 *Disturbr* represents a significant new option for many ecologists interested in change  
480 detection at local and regional scales. Additionally, as the approach does not depend on any  
481 one type of data, multiple data types and resolutions can easily be used depending on the  
482 desired results. While we used NDVI as the spectral index for this analysis, other studies

483 have demonstrated that shortwave infrared (SWIR)-based indices may be more effective for  
484 disturbance detection (Schultz et al. 2016, Cohen et al. 2018). These indices could easily  
485 be applied to this approach. Additional increases in accuracy might also be achieved by  
486 integrating variable summaries of additional factors such as topographic wetness index or  
487 land surface temperature.

488 While *disturbr* demonstrates the potential for improvement in current disturbance detec-  
489 tion and attribution approaches, there are several limitations to the current analysis. First,  
490 our results were limited by the use of only summertime NDVI values for the analysis. We  
491 masked out clouds, cloud shadows, and other areas marked as being of low quality, but this  
492 resulted in a number of pixels with large chunks of missing data. For this study, we filled in  
493 these pixels using mean NDVI over the pixel time series. This approach led to flattened time  
494 series in which trends in NDVI over time were less visible and therefore leading to potential  
495 omission errors. The use of spatial information mitigated this problem somewhat, but a  
496 better method for the interpolation of missing data points, or the use of better-prepared  
497 data (e.g., Robinson et al. 2017), would further improve results. A separate issue with this  
498 approach is the need for good training data for both the detection and attribution models.  
499 Most disturbance models require some tuning for each region in which they are applied,  
500 so this is not a unique issue. However, *disturbr* relies solely on those training data and is  
501 therefore capable of producing both extremely good or extremely poor results depending on  
502 the abilities of the trainer or the availability of training data. When using the pipeline as  
503 described here, it is necessary to become familiar with the typical characteristics of the re-  
504 gion and to train a sufficient number of points so that a few mistaken training points do not  
505 have too strong an influence on the results. Further work is needed to determine both the  
506 best density of training points and the sensitivity of the models to the presence of incorrect  
507 training points (e.g., Rogan et al. 2008).

508    **5 Conclusion**

509    We introduced *disturbr*, a new disturbance detection and attribution framework that  
510    combines POI, NPI, and machine learning in an attempt to improve detection and attribution  
511    accuracy, transferability, and efficiency. We found that while accuracy still varied among  
512    regions and disturbance types, the false positive and negative rates using this new method  
513    were similar to or better than those from strictly temporal approaches. In addition, we found  
514    that the variables important for disturbance detection and attribution varied among regions.  
515    POI variables were more important for detection, while NPI variables gained importance for  
516    attribution. However, detection models that incorporated NPI were more accurate than those  
517    with POI alone. While some disturbance characteristics (e.g., POI minimum loess slope)  
518    were important across all regions, the overall lack of correspondence in variable importance  
519    among regions suggests that both disturbance characteristics and the environment in which  
520    they occur vary considerably by forest type and local environmental conditions. These  
521    differences may explain why other algorithms are very accurate in one region, but lose  
522    accuracy when transferred to other regions. The *disturbr* framework developed here is most  
523    useful when applied to local- to regional-scale studies and is freely available on GitHub  
524    (<https://github.com/AnnieCooper/disturbr-public>) as a set of scripts and functions.

525    **6 Acknowledgements**

526    This work was funded by a NASA Earth and Space Science fellowship to ACS (#NNX15AN16H).  
527    ACS designed and developed the approach, with feedback from APB and ZHL. ACS, APB,  
528    PLZ, and ZHL contributed to the interpretation of results. ACS wrote the manuscript with  
529    contributions from all authors. ACS and PLZ provided computational resources. We would  
530    also like to thank S. Dobrowski, Z. Holden, E. Landguth, S. Smith, and the Ballantyne and  
531    Zarnetske labs for critical feedback on the concept and manuscript.

532 **References**

- 533 Breiman, L., 2001. Random forests. Machine Learning 45, 5–32. doi:10.1023/a:  
534 1010933404324.
- 535 Chander, G., Markham, B.L., Helder, D.L., 2009. Summary of current radiometric cali-  
536 bration coefficients for landsat mss, tm, etm+, and eo-1 ali sensors. Remote Sensing of  
537 Environment 113, 893–903. doi:10.1016/j.rse.2009.01.007.
- 538 Cohen, J., 1968. Weighted kappa - nominal scale agreement with provision for scaled dis-  
539 agreement or partial credit. Psychological Bulletin 70, 213–. doi:10.1037/h0026256.
- 540 Cohen, W.B., Healey, S.P., Yang, Z., Stehman, S.V., Brewer, C.K., Brooks, E.B., Gorelick,  
541 N., Huang, C., Hughes, M.J., Kennedy, R.E., Loveland, T.R., Moisen, G.G., Schroeder,  
542 T.A., Vogelmann, J.E., Woodcock, C.E., Yang, L., Zhu, Z., 2017. How similar are forest  
543 disturbance maps derived from different landsat time series algorithms? Forests 8. doi:10.  
544 3390/f8040098.
- 545 Cohen, W.B., Yang, Z., Heale, S.P., Kennedy, R.E., Gorelic, N., 2018. A landtrendr multi-  
546 spectral ensemble for forest disturbance detection. Remote Sensing of Environment 205,  
547 131–140. doi:10.1016/j.rse.2017.11.015.
- 548 Cohen, W.B., Yang, Z., Kennedy, R., 2010. Detecting trends in forest disturbance and  
549 recovery using yearly landsat time series: 2. timesync - tools for calibration and validation.  
550 Remote Sensing of Environment 114, 2911–2924. doi:10.1016/j.rse.2010.07.010.
- 551 Cooper, L.A., Ballantyne, A.P., Holden, Z.A., Landguth, E.L., 2017. Disturbance im-  
552 pacts on land surface temperature and gross primary productivity in the western united  
553 states. Journal of Geophysical Research-Biogeosciences 122, 930–946. doi:10.1002/  
554 2016jg003622.

- 555 Curtis, P.G., Slay, C.M., Harris, N.L., Tyukavina, A., Hansen, M.C., 2018. Classifying  
556 drivers of global forest loss. *Science* 361, 1108–1111.
- 557 Foster, D., Swanson, F., Aber, J., Burke, I., Brokaw, N., Tilman, D., Knapp, A., 2003. The  
558 importance of land-use legacies to ecology and conservation. *BioScience* 53, 77–88.
- 559 Fotheringham, A.S., Charlton, M., Brunsdon, C., 1996. The geography of parameter space:  
560 An investigation of spatial non-stationarity. *International Journal of Geographical Infor-*  
561 *mation Systems* 10, 605–627. doi:10.1080/02693799608902100.
- 562 Frissell, S.S.J., 1973. The importance of fire as a natural ecological factor in itasca state  
563 park minnesota. *Quaternary Research (Orlando)* 3, 397–407. doi:10.1016/0033-5894(73)  
564 90005-7.
- 565 Gomez, C., White, J.C., Wulder, M.A., 2011. Characterizing the state and processes of  
566 change in a dynamic forest environment using hierarchical spatio-temporal segmentation.  
567 *Remote Sensing of Environment* 115, 1665–1679. doi:10.1016/j.rse.2011.02.025.
- 568 Google, 2019. Google earth pro.
- 569 Google, n.d. Google maps. URL: [maps.google.com](https://maps.google.com).
- 570 Gorelick, N., Hancher, M., Dixon, M., Ilyushchenko, S., Thau, D., Moore, R., 2017. Google  
571 earth engine: Planetary-scale geospatial analysis for everyone. *Remote Sensing of Envi-*  
572 *ronment* 202, 18–27.
- 573 Hansen, M., Potapov, P., Margono, B., Stehman, S., Turubanova, S., Tyukavina, A., 2014.  
574 Response to comment on "high-resolution global maps of 21st-century forest cover change".  
575 *Science* 344. doi:10.1126/science.1248817.
- 576 Hansen, M.C., Potapov, P.V., Moore, R., Hancher, M., Turubanova, S.A., Tyukavina, A.,  
577 Thau, D., Stehman, S.V., Goetz, S.J., Loveland, T.R., Kommareddy, A., Egorov, A.,

- 578 Chini, L., Justice, C.O., Townshend, J.R.G., 2013. High-resolution global maps of 21st-  
579 century forest cover change. *Science* 342, 850–853. doi:10.1126/science.1244693.
- 580 Healey, S.P., Cohen, W.B., Yang, Z., Brewer, C.K., Brooks, E.B., Gorelick, N., Hernandez,  
581 A.J., Huang, C., Hughes, M.J., Kennedy, R.E., Loveland, T.R., Moisen, G.G., Schroeder,  
582 T.A., Stehman, S.V., Vogelmann, J.E., Woodcock, C.E., Yang, L., Zhu, Z., 2018. Mapping  
583 forest change using stacked generalization: An ensemble approach. *Remote Sensing of*  
584 *Environment* 204, 717–728. doi:10.1016/j.res.2017.09.029.
- 585 Huang, C., Song, K., Kim, S., Townshend, J.R.G., Davis, P., Masek, J.G., Goward, S.N.,  
586 2008. Use of a dark object concept and support vector machines to automate forest cover  
587 change analysis. *Remote Sensing of Environment* 112, 970–985. doi:10.1016/j.rse.2007.  
588 07.023.
- 589 Kennedy, R.E., Yang, Z., Braaten, J., Copass, C., Antonova, N., Jordan, C., Nelson, P.,  
590 2015. Attribution of disturbance change agent from landsat time-series in support of  
591 habitat monitoring in the puget sound region, usa. *Remote Sensing of Environment* 166,  
592 271–285. doi:10.1016/j.rse.2015.05.005.
- 593 Kennedy, R.E., Yang, Z., Cohen, W.B., 2010. Detecting trends in forest disturbance and re-  
594 covery using yearly landsat time series: 1. landtrendr - temporal segmentation algorithms.  
595 *Remote Sensing of Environment* 114, 2897–2910. doi:10.1016/j.rse.2010.07.008.
- 596 Kuhn, M., 2015. caret: Classification and regression training. *Astrophysics Source Code*  
597 *Library*.
- 598 Liaw, A., Wiener, M., et al., 2002. Classification and regression by randomforest. *R news* 2,  
599 18–22.
- 600 Lippitt, C.D., Rogan, J., Li, Z., Eastman, J.R., Jones, T.G., 2008. Mapping selective logging  
601 in mixed deciduous forest: A comparison of machine learning algorithms. *Photogrammet-  
602 ric Engineering and Remote Sensing* 74, 1201–1211. doi:10.14358/pers.74.10.1201.

- 603 Liu, Z., Ballantyne, A.P., Cooper, L.A., 2019. Biophysical feedback of global forest fires on  
604 surface temperature. *Nature Communications* 10. doi:10.1038/s41467-018-08237-z.
- 605 Maness, H., Kushner, P.J., Fung, I., 2013. Summertime climate response to mountain  
606 pine beetle disturbance in british columbia. *Nature Geoscience* 6, 65–70. doi:10.1038/  
607 ngeo1642.
- 608 Masek, J.G., Goward, S.N., Kennedy, R.E., Cohen, W.B., Moisen, G.G., Schleeweis, K.,  
609 Huang, C., 2013. United states forest disturbance trends observed using landsat time  
610 series. *Ecosystems* 16, 1087–1104.
- 611 McDowell, N.G., Coops, N.C., Beck, P.S.A., Chambers, J.Q., Gangodagamage, C., Hicke,  
612 J.A., Huang, C.y., Kennedy, R., Kroscheck, D.J., Litvak, M., Meddens, A.J.H., Muss, J.,  
613 Negron-Juarez, R., Peng, C., Schwantes, A.M., Swenson, J.J., Vernon, L.J., Williams,  
614 A.P., Xu, C., Zhao, M., Running, S.W., Allen, C.D., 2015. Global satellite monitoring  
615 of climate-induced vegetation disturbances. *Trends in Plant Science* 20, 114–123. doi:10.  
616 1016/j.tplants.2014.10.008.
- 617 McIntire, E.J., Fajardo, A., 2009. Beyond description: the active and effective way to infer  
618 processes from spatial patterns. *Ecology* 90, 46–56.
- 619 Mildrexler, D.J., Zhao, M.S., Heinsch, F.A., Running, S.W., 2007. A new satellite-based  
620 methodology for continental-scale disturbance detection. *Ecological Applications* 17, 235–  
621 250. doi:10.1890/1051-0761(2007)017[0235:ansmfc]2.0.co;2.
- 622 Morehouse, K., Johns, T., Kaye, J., Kaye, A., 2008. Carbon and nitrogen cycling immediately  
623 following bark beetle outbreaks in southwestern ponderosa pine forests. *Forest Ecology  
624 and Management* 255, 2698–2708. doi:10.1016/j.foreco.2008.01.050.
- 625 Niemelä, J., 1999. Management in relation to disturbance in the boreal forest. *Forest Ecology  
626 and Management* 115, 127–134.

- 627 Pal, M., Mather, P.M., 2003. An assessment of the effectiveness of decision tree methods  
628 for land cover classification. *Remote Sensing of Environment* 86, 554–565. doi:10.1016/  
629 s0034-4257(03)00132-9.
- 630 Peterson, D.L., Schreiner, E.G., Buckingham, N.M., 1997. Gradients, vegetation and cli-  
631 mate: spatial and temporal dynamics in the olympic mountains, usa. *Global Ecology and*  
632 *Biogeography Letters* 6, 7–17. doi:10.2307/2997523.
- 633 Rich, R.L., Frelich, L., Reich, P.B., Bauer, M.E., 2010. Detecting wind disturbance severity  
634 and canopy heterogeneity in boreal forest by coupling high-spatial resolution satellite im-  
635 agery and field data. *Remote Sensing of Environment* 114, 299–308. doi:10.1016/j.rse.  
636 2009.09.005.
- 637 Robinson, N., Allred, B., Jones, M., Moreno, A., Kimball, J., Naugle, D., Erickson, T.,  
638 Richardson, A., 2017. A dynamic landsat derived normalized difference vegetation index  
639 (ndvi) product for the conterminous united states. *Remote Sensing* 9, 863.
- 640 Rogan, J., Franklin, J., Stow, D., Miller, J., Woodcock, C., Roberts, D., 2008. Mapping  
641 land-cover modifications over large areas: A comparison of machine learning algorithms.  
642 *Remote Sensing of Environment* 112, 2272–2283. doi:10.1016/j.rse.2007.10.004.
- 643 Schroeder, T.A., Schleeweis, K.G., Moisen, G.G., Toney, C., Cohen, W.B., Freeman, E.A.,  
644 Yang, Z., Huang, C., 2017. Testing a landsat-based approach for mapping disturbance  
645 causality in us forests. *Remote Sensing of Environment* 195, 230–243. doi:10.1016/j.  
646 rse.2017.03.033.
- 647 Schultz, M., Clevers, J.G., Carter, S., Verbesselt, J., Avitabile, V., Quang, H.V., Herold,  
648 M., 2016. Performance of vegetation indices from landsat time series in deforestation  
649 monitoring. *International journal of applied earth observation and geoinformation* 52,  
650 318–327.

- 651 Shimizu, K., Ahmed, O.S., Ponce-Hernandez, R., Ota, T., Win, Z.C., Mizoue, N., Yoshida,  
652 S., 2017. Attribution of disturbance agents to forest change using a landsat time series  
653 in tropical seasonal forests in the bago mountains, myanmar. Forests 8. doi:10.3390/  
654 f8060218.
- 655 Smucker, K.M., Hutto, R.L., Steele, B.M., 2005. Changes in bird abundance after wildfire:  
656 Importance of fire severity and time since fire. Ecological Applications 15, 1535–1549.  
657 doi:10.1890/04-1353.
- 658 Song, X.P., Hansen, M.C., Stehman, S.V., Potapov, P.V., Tyukavina, A., Vermote, E.F.,  
659 Townshend, J.R., 2018. Global land change from 1982 to 2016. Nature 560, 639.
- 660 Sousa, W.P., 1984. The role of disturbance in natural communities. Annual Review of  
661 Ecology and Systematics 15, 353–391.
- 662 Team, R.C., 2017. R: A language and environment for statistical computing. URL: <http://www.R-project.org>.
- 664 Therneau, T., Atkinson, B., Ripley, B., 2017. rpart: Recursive partitioning and regression  
665 trees.
- 666 Tropek, R., Sedlacek, O., Beck, J., Keil, P., Musilova, Z., Simova, I., Storch, D., 2014.  
667 Comment on "high-resolution global maps of 21st-century forest cover change". Science  
668 344. doi:10.1126/science.1248753.
- 669 Verbesselt, J., Hyndman, R., Newnham, G., Culvenor, D., 2010. Detecting trend and sea-  
670 sonal changes in satellite image time series. Remote Sensing of Environment 114, 106–115.  
671 doi:10.1016/j.rse.2009.08.014.
- 672 Verbesselt, J., Zeileis, A., Herold, M., 2012. Near real-time disturbance detection using  
673 satellite image time series. Remote Sensing of Environment 123, 98–108. doi:10.1016/j.  
674 rse.2012.02.022.

- 675 Wan, S.Q., Hui, D.F., Luo, Y.Q., 2001. Fire effects on nitrogen pools and dynamics in  
676 terrestrial ecosystems: A meta-analysis. Ecological Applications 11, 1349–1365. doi:10.  
677 1890/1051-0761(2001)011[1349:feonpa]2.0.co;2.
- 678 Yensen, E., Quinney, D.L., Johnson, K., Timmerman, K., Steenhof, K., 1992. Fire, vegeta-  
679 tion changes, and population fluctuations of townsend ground-squirrels. American Midland  
680 Naturalist 128, 299–312. doi:10.2307/2426464.
- 681 Zhao, F., Huang, C., Goward, S.N., Schleeweis, K., Rishmawi, K., Lindsey, M.A., Denning,  
682 E., Keddell, L., Cohen, W.B., Yang, Z., Dungan, J.L., Michaelis, A., 2018. Development  
683 of landsat-based annual us forest disturbance history maps (1986-2010) in support of the  
684 north american carbon program (nACP). Remote Sensing of Environment 209, 312–326.  
685 doi:10.1016/j.rse.2018.02.035.
- 686 Zhao, F., Huang, C., Zhu, Z., 2015. Use of vegetation change tracker and support vector  
687 machine to map disturbance types in greater yellowstone ecosystems in a 1984-2010 landsat  
688 time series. Ieee Geoscience and Remote Sensing Letters 12, 1650–1654. doi:10.1109/  
689 lgrs.2015.2418159.
- 690 Zhu, Z., Woodcock, C.E., Olofsson, P., 2012. Continuous monitoring of forest disturbance  
691 using all available landsat imagery. Remote Sensing of Environment 122, 75–91. doi:10.  
692 1016/j.rse.2011.10.030.